

# Oxidation Behavior of NiTi Alloy Under Low Oxygen Partial Pressure

Shao Mingzeng<sup>1,2</sup>, Zhao Xu<sup>1,2</sup>, Yang Hongbo<sup>1,3</sup>

<sup>1</sup> Xi'an University of Architecture and Technology, Xi'an 710055, China; <sup>2</sup> Key Laboratory of Gold and Resources of Shaanxi Province, Xi'an 710055, China; <sup>3</sup> Research Centre of Metallurgical Engineering & Technology of Shaanxi Province, Xi'an 710055, China

**Abstract:** The isothermal oxidation behavior of NiTi alloy in H<sub>2</sub>-H<sub>2</sub>O in the temperature range from 400 °C to 700 °C was studied. The results show that the oxidation rate of the NiTi alloy follows cubic laws, and the activation energy for the oxidation of the alloy is determined to be 127.52 kJ/mol. The surface Ni content is significantly reduced by selective oxidation. For the sample oxidized at 400 °C, the morphology is different from those formed at high temperatures. For the samples oxidized at 500, 600, and 700 °C, the oxide scales show two morphologies, which consist of cubic grains and oxide whiskers. Cross-section analyses show that the oxide scales consist of an outer TiO<sub>2</sub> layer and an inner Ni<sub>3</sub>Ti layer. Voids form near the interface of the two layers.

**Key words:** NiTi alloy; selective oxidation; low oxygen partial pressure; TiO<sub>2</sub>

NiTi alloys with nearly equiatomic nickel-to-titanium ratios are widely used in biomedical applications because of their unique shape-memory properties and good corrosion resistance<sup>[1]</sup>. However, the higher concentration of Ni in the alloy increases the risks of allergy and adverse reactions<sup>[2,3]</sup>.

A high-purity TiO<sub>2</sub> layer has been proven to be a reliable barrier against Ni release<sup>[4-6]</sup>. To synthesize such TiO<sub>2</sub> layer on the alloy, several studies<sup>[7-9]</sup> have focused on the isothermal oxidation behavior of NiTi in air and oxygen. The oxide scale formed in such atmosphere is always mixed with Ni or NiO<sup>[4,10-12]</sup> and has demonstrated a high spallation tendency<sup>[13]</sup>, thereby reducing the barrier performance of the oxide scale.

A promising method to reduce the Ni content of the oxide scale is an oxidation process under low oxygen partial pressure. The oxygen affinity of Ti is higher than that of Ni. Therefore, under very low oxygen partial pressure, selective oxidation of Ti is possible to realize, and oxidation of Ni can be inhibited. After the oxidation process, a titanium-rich oxide scale will form on the alloy. To obtain low values of oxygen partial pressure, a suitable mixture of H<sub>2</sub> and H<sub>2</sub>O is consistently used<sup>[14,15]</sup>. Several studies on the oxidation

behavior of FeCr<sup>[16]</sup>, NiCr<sup>[17,18]</sup>, and FeCrNi<sup>[19]</sup> under low oxygen partial pressure have been conducted. However, little is known about the oxidation behavior of NiTi alloy under low oxygen partial pressure. Therefore, in this paper, the oxidation behavior of NiTi alloy in H<sub>2</sub>-H<sub>2</sub>O is presented.

## 1 Experiment

The material used in the experiment is a commercial hot-rolled NiTi plate with nominal composition of 50.2 at% Ti and 49.8 at% Ni. The specimens were cut from the plate to a size of 20 mm×10 mm×2 mm, with a hole of 1.6 mm in diameter near the center of an edge. The samples were ground on emery papers up to 1000 grit, washed in acetone, and dried before the oxidation test.

Oxidation experiments were performed in the equipment (Fig.1). The gas mixture of hydrogen and water vapor was generated by flowing hydrogen through distilled water ( $T_{\text{bubbler}}=10\text{ }^{\circ}\text{C}$ ). Isothermal oxidation was conducted at temperatures of 400, 500, 600, and 700 °C for 10 h. The mass gain of the specimens was recorded as a function of time by the thermal balance (Therm HM) during oxidation. After the

Received date: April 28, 2017

Foundation item: The Natural Science Basic Research Program of Shaanxi Province (2013JQ6017); Foundation of Xi'an University of Architecture and Technology (RC1329)

Corresponding author: Shao Mingzeng, Ph. D., Lecturer, School of Metallurgical Engineering, Xi'an University of Architecture and Technology, Xi'an 710055, P. R. China, Tel: 0086-29-82202923, E-mail: smz516@163.com

Copyright © 2018, Northwest Institute for Nonferrous Metal Research. Published by Elsevier BV. All rights reserved.

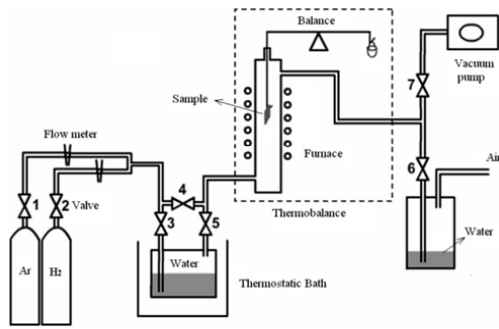


Fig.1 Schematic of test oxidation equipment

isothermal oxidation, the oxidized specimens were cooled to room temperature in the furnace.

After oxidation, the phase structures of the oxide scales were identified by X-ray diffraction (XRD, Bruker D8 ADVANCE). The surface and cross section morphologies of samples were analyzed using scanning electron microscopy (SEM, QUANTA 200) equipped with an energy-dispersive X-ray spectroscopy (EDS, EDAX-Genesis Apex) system.

## 2 Results and Discussion

### 2.1 Oxidation kinetics

The mass-change curves of the samples oxidized at 400, 500, 600, and 700 °C in H<sub>2</sub>-H<sub>2</sub>O are plotted in Fig.2. The oxidation rate increases with temperature increasing. After oxidation for 10 h, the mass gains are 0.073, 0.142, 0.340, and 0.760 mg/cm<sup>2</sup> for the samples oxidized at 400, 500, 600, and

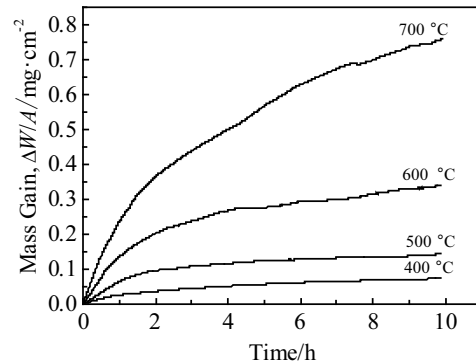


Fig.2 Mass gains versus time for isothermal oxidation of NiTi alloy at different temperatures

700 °C, respectively.

Fig.3 shows the plot of  $(W/A)^3$  versus time corresponding to the thermogravimetric analysis shown in Fig.2. As shown in the figure, a nearly linear relationship between  $(W/A)^3$  and time is observed, which indicates that the kinetics follows cubic law.

The values of  $K_p$  were obtained from the slope of the  $(W/A)^3$  versus time plots. The activation energy of oxidation was calculated using the Arrhenius equation as follows:

$$K_p = A \exp(-Q/RT) \quad (1)$$

Table 1 lists the cubic rate constants  $K_p$  at the four temperatures and the activation energy of oxidation. The rate constant increases as the oxidation temperature increases. The

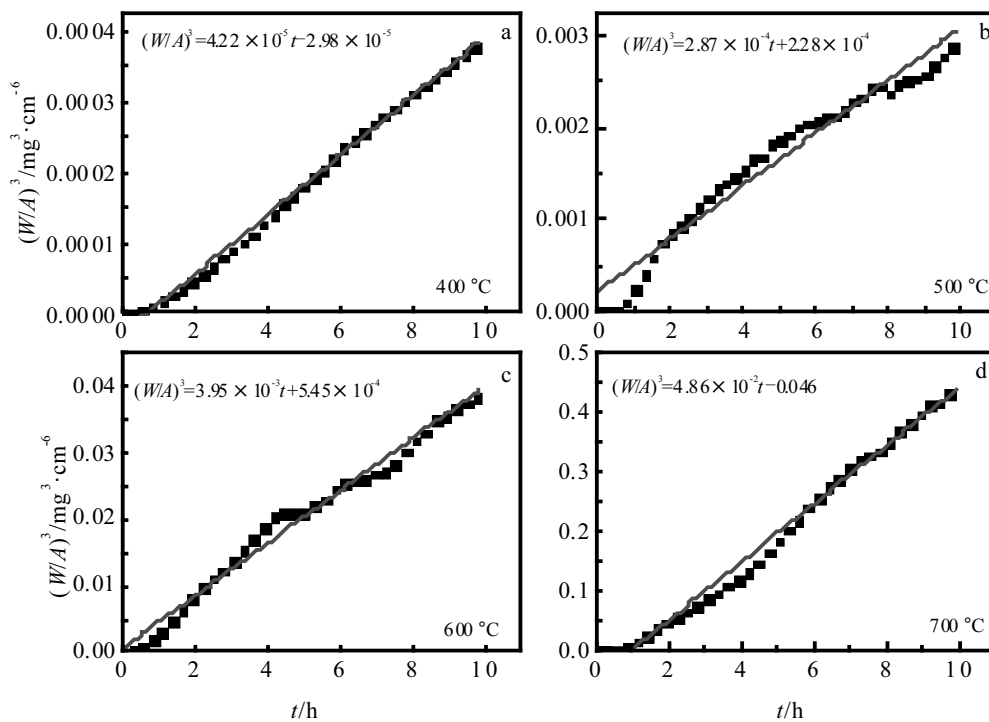


Fig.3  $(W/A)^3$  versus time for isothermal oxidation of NiTi alloy at 400 °C (a), 500 °C (b), 600 °C (c), and 700 °C (d)

**Table 1 Cubic rate constants and activation energy of oxidation for NiTi alloy**

Temperature/°C	$K_p/\text{mg}^3\cdot\text{cm}^{-6}\cdot\text{h}^{-1}$	$Q/\text{kJ}\cdot\text{mol}^{-1}$
400	$4.22\times 10^{-5}$	127.52
500	$2.87\times 10^{-4}$	
600	$3.95\times 10^{-3}$	
700	$4.86\times 10^{-2}$	

activation energy is determined to be 127.52 kJ/mol.

## 2.2 Phase composition

Fig.4 shows the XRD patterns of NiTi samples oxidized in  $\text{H}_2\text{-H}_2\text{O}$  at 400, 500, 600, and 700 °C. After oxidation at 400 °C, the XRD pattern shows only NiTi peaks. No oxide peaks are observed, indicating that the scale formed at this temperature is too thin to be detected. For the samples oxidized at 500, 600, and 700 °C, rutile  $\text{TiO}_2$  peaks are observed. In addition, the intensities of the peaks become stronger as the oxidation temperature increases. This result implies that the growth of  $\text{TiO}_2$  dominates the oxidation behavior.  $\text{Ni}_3\text{Ti}$  peaks are also observed for specimens oxidized at 500, 600, and 700 °C. However, the intensities of the peaks gradually decrease with the increasing oxidation temperature. This finding indicates that the  $\text{TiO}_2$  oxide scale becomes thicker as the temperature increases, which may prevent the  $\text{Ni}_3\text{Ti}$  phase from being detected.

## 2.3 Morphology and composition

The surface morphologies of NiTi specimens after oxidation are shown in Fig.5. Oxide scales grow and cover the

whole surface of the samples. No cracks or spallation appear on the scales, indicating that the scales adhere well to the base alloy. For the sample oxidized at 400 °C, the scale is uneven. Scratch marks formed during the sample preparation process can be observed, suggesting that the oxide layer is very thin. The samples oxidized at 500, 600, and 700 °C show two morphologies, which consist of cubic grains and oxide whiskers. The sizes of the cubic grains and the whiskers increase with the oxidation temperature increasing. Previous studies<sup>[8,10,13]</sup> showed that the oxidation of NiTi alloy in dry oxygen only produced films with densely packed  $\text{TiO}_2$  and

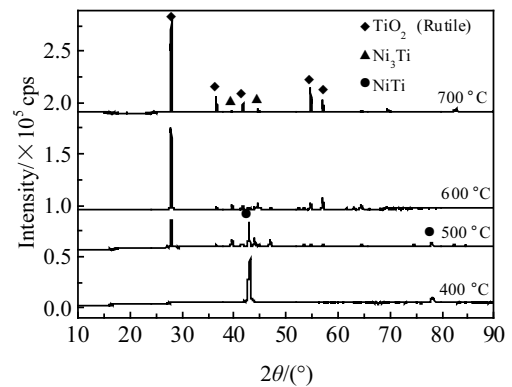


Fig.4 XRD patterns of NiTi samples after oxidation for 10 h in  $\text{H}_2\text{-H}_2\text{O}$  at 400, 500, 600, and 700 °C

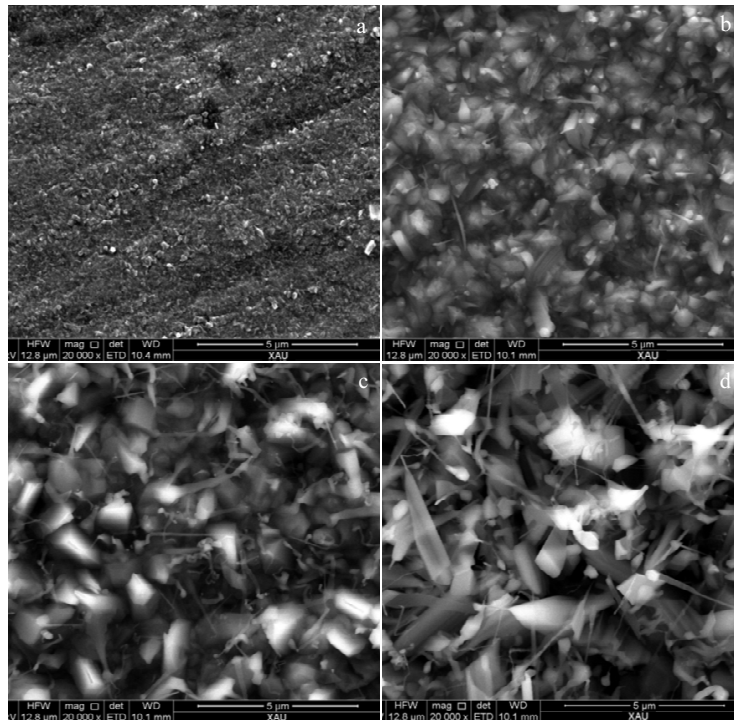


Fig.5 Surface morphologies of NiTi oxidized in  $\text{H}_2\text{-H}_2\text{O}$  at 400 °C (a), 500 °C (b), 600 °C (c), and 700 °C (d)

NiTiO<sub>3</sub> grains, and no oxide whiskers formed. Oxide whiskers were commonly observed when water vapor was present in the environment<sup>[14,15,20]</sup>. The generally accepted mechanism of oxide whisker formation was proposed by Raynaud and Rapp<sup>[21]</sup>; they suggested that the whiskers arise from dislocations in the oxide and involve a tunnel acting as high-diffusivity paths. They also suggested that the dissociation of H<sub>2</sub>O molecules is generally faster than that of O<sub>2</sub> molecules at the tip of the whisker. Under the influence of these factors, the growth of the oxide in the direction of the whisker axis is much greater than its lateral growth.

The chemical composition of the oxide scale was analyzed by EDS, and the results are listed in Table 2. The Ni content of the sample oxidized at 400 °C is very high, probably because the oxide scale formed at this temperature is very thin, and the composition of the base alloy is detected. For the samples oxidized at 500, 600, and 700 °C, their composition is similar, which mainly consists of Ti and O. Furthermore, the atomic ratio of Ti to O is close to 1:2, which is consistent with the stoichiometric ratio of TiO<sub>2</sub>. Although the alloys contain a large amount of Ni, no Ni is detected in the scale. This finding reflects the difference in the oxygen affinity between Ti and Ni.

The oxygen partial pressure is calculated using the following equations<sup>[22]</sup>:

$$\lg(P_{\text{H}_2\text{O}}) = 7.58 \times \frac{T_{\text{bubbler}}}{240 + T_{\text{bubbler}}} - 2.22 \quad (2)$$

$$\frac{1}{2} \lg(P_{\text{O}_2}) = 3.0 - \frac{13088}{T} + \lg\left(\frac{P_{\text{H}_2\text{O}}}{P_{\text{H}_2}}\right) \quad (3)$$

where  $P_{\text{H}_2}$ ,  $P_{\text{O}_2}$ , and  $P_{\text{H}_2\text{O}}$  represent the partial pressures of hydrogen, oxygen, and water vapor, respectively.  $T_{\text{bubbler}}$  is the temperature of the water, and  $T$  is the temperature of oxidation. The calculated oxygen partial pressures at different temperatures are listed in Table 3. The oxygen partial pressures for the formation of TiO<sub>2</sub> ( $P_{\text{Ti/TiO}_2}$ ) and NiO ( $P_{\text{Ni/NiO}}$ ) by the reaction:



and



were extrapolated from the data given by Inden<sup>[23]</sup>. The results are also listed in Table 3.

As presented in Table 3, the oxygen partial pressures  $P_{\text{O}_2}$  at different oxidation temperatures are much lower than the required oxygen partial pressures for Ni oxidation, but the values are higher than the required oxygen partial pressure for Ti oxidation. In such condition, Ni remains in metallic state after 10 h exposure to the environment, whereas Ti is selectively oxidized, and oxide scales rich in Ti are formed.

#### 2.4 Cross section

The cross-sectional microstructures of the NiTi samples are shown in Fig.6. For the sample oxidized at 400 °C, no visible oxide is observed by SEM because the oxide layer is too thin to be detected. Oxide scales are obvious on the samples oxidized at 500, 600, and 700 °C. All the scales are composed of two layers and the thickness increases with temperature increasing. EDS analyses indicate that the gray external layers are rich in Ti and O. The bright layers beneath the structure are rich in Ni and Ti. Combination of EDS and XRD analyses show that the outer layers are composed of TiO<sub>2</sub>, and the beneath layers are composed of Ni<sub>3</sub>Ti. According to the thermal dynamic calculation, when the oxidation occurs, the Ti in the NiTi alloy is selectively oxidized, and TiO<sub>2</sub> forms preferentially on the surfaces. With the outward diffusion of Ti, the Ni<sub>3</sub>Ti phases develop beneath the TiO<sub>2</sub> layer because of the depletion of Ti.

Some voids are found at the bottom of the TiO<sub>2</sub> layer and on the top of the Ni<sub>3</sub>Ti layer. The size and density of voids depend on the temperature. Similar voids were also reported in previous investigations<sup>[7,24]</sup>. Chu<sup>[7]</sup> suggested that the voids at the bottom of the TiO<sub>2</sub> scale are possibly formed as a result of the difference between the vertical and lateral growth rates during the initial stages of the oxide scale formation. The formation of pores in the Ni<sub>3</sub>Ti layer is related to the Kirkendall effect. When the Ti atoms diffuse away from the NiTi matrix, vacancies are created. Along with the heating process, vacancies may collect to form pores.

Previous studies<sup>[9,11,25]</sup> showed that the double-oxide NiTiO<sub>3</sub> was always formed beneath or within the TiO<sub>2</sub> layer for the samples oxidized in air. In the present study, no NiTiO<sub>3</sub> oxides are found. Zeng<sup>[12]</sup> suggested that the NiTiO<sub>3</sub> was formed by NiO reacting with TiO<sub>2</sub>. In the present study, the oxygen pressure is not high enough to form thermodynamically stable oxides of Ni, which prevents the formation of NiTiO<sub>3</sub>.

**Table 2 Chemical composition of the oxide scale surface (at%)**

Temperature/°C	O	Ti	Ni
400	33.16	32.59	34.25
500	65.80	34.20	-
600	65.46	34.54	-
700	65.24	34.76	-

**Table 3 Calculated result of  $P_{\text{O}_2}$ ,  $P_{\text{Ni/NiO}}$  and  $P_{\text{Ti/TiO}_2}$  at different temperatures**

Temperature/°C	$P_{\text{O}_2}$	$P_{\text{Ni/NiO}}$	$P_{\text{Ti/TiO}_2}$
400	$2.13 \times 10^{-42}$	$2.18 \times 10^{-28}$	$2.58 \times 10^{-61}$
500	$2.26 \times 10^{-37}$	$1.77 \times 10^{-23}$	$2.62 \times 10^{-52}$
600	$1.69 \times 10^{-33}$	$1.07 \times 10^{-17}$	$2.30 \times 10^{-45}$
700	$2.03 \times 10^{-30}$	$1.09 \times 10^{-16}$	$7.55 \times 10^{-40}$

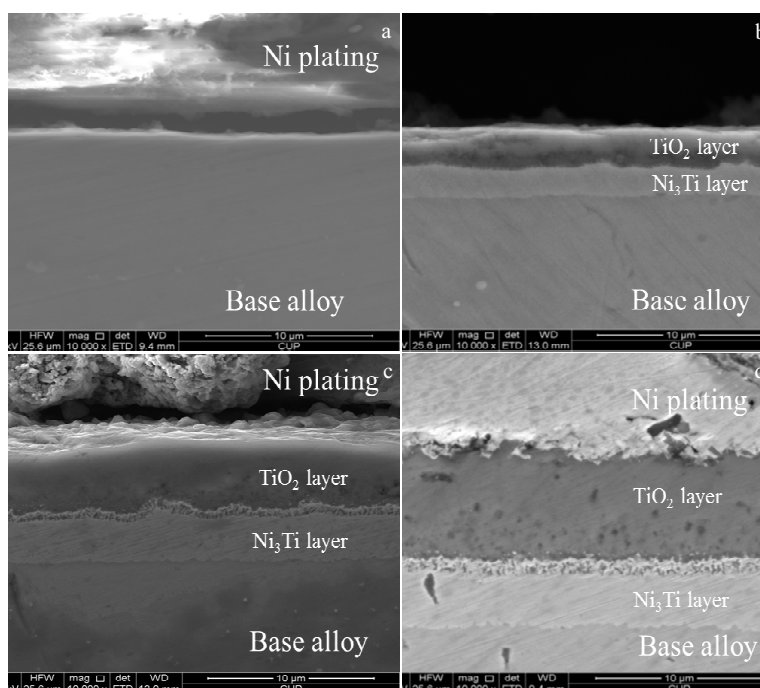


Fig.6 Cross-sectional microstructures of NiTi sample oxidized at 400 °C (a), 500 °C (b), 600 °C (c), and 700 °C (d)

### 3 Conclusions

1) The oxidation rate of the NiTi alloy at 400, 500, 600, and 700 °C follows cubic laws, and the activation energy for the oxidation of the alloy is determined to be 127.52 kJ/mol.

2) For the samples oxidized at 500, 600, and 700 °C, the surface Ni content is significantly reduced by selective oxidation, and the oxide scales show two morphologies, which consist of cubic grains and oxide whiskers.

3) The scales exhibit two-layer structures. The outer layer of the scale is composed of  $\text{TiO}_2$ , whereas the beneath layer is composed of  $\text{Ni}_3\text{Ti}$ . Voids form near the interface of the two layers.

### References

- Otsuka K, Ren X. *Progress in Materials Science*[J], 2005, 50(5): 511
- Wataha J C, O'Dell N L, Singh B B et al. *Journal of Biomedical Materials Research*[J], 2001, 58(5): 537
- Wang Shengnan, Cui Yue, Yuan Zhishan et al. *Rare Metal Materials and Engineering*[J], 2015, 44: 509 (in Chinese)
- Shabalovskaya S A, Tian H, Anderegg J W et al. *Biomaterials*[J], 2009, 30(4): 468
- Yuan B, Li H, Gao Y et al. *Science China Technological Sciences*[J], 2012, 55(2): 437
- Heßing C, Pohl M. *International Journal of Materials Research*[J], 2009, 100(8): 1099
- Chu C L, Wu S K, Yen Y C. *Materials Science and Engineering A*[J], 2006, 216(1-2): 193
- Vojtěch D, Novák P, Novák M et al. *Intermetallics*[J], 2008, 16(3): 424
- Smialek J L, Garg A, Rogers R B et al. *Metallurgical & Materials Transactions A*[J], 2012, 43(7): 2325
- Firstov G S, Vitchev R G, Kumar H et al. *Biomaterials*[J], 2002, 23(24): 4863
- Xu J, Zhao X, Gong S. *Transactions of Nonferrous Metals Society of China*[J], 2006, 16: 31
- Zeng C L, Li M C, Liu G Q et al. *Oxidation of Metals*[J], 2002, 58(1-2): 171
- Xu C H, Ma X Q, Shi S Q et al. *Materials Science and Engineering A*[J], 2004, 371(1-2): 45
- Mikkelsen L, Linderoth S. *Materials Science and Engineering A*[J], 2003, 361(1-2): 198
- Othman N K, Othman N, Zhang J et al. *Corrosion Science*[J], 2009, 51(12): 3039
- Horita T, Xiong Y, Yamaji K et al. *Fuel Cells*[J], 2002, 2(3-4): 189
- Zurek J, Young D J, Essuman E et al. *Materials Science and Engineering A*[J], 2008, 477(1-2): 259
- Hänsel M, Garcia-Fresnillo L, Tobing S L et al. *Materials at High Temperatures*[J], 2012, 29(3): 187
- Rabbani F, Ward L P, Strafford K N. *Oxidation of Metals*[J], 2000, 54(1-2): 139
- Chandra K, Kranzmann A, Neumann R S et al. *Oxidation of Metals*[J], 2015, 84(3-4): 463
- Raynaud G M, Rapp R A. *Oxidation of Metals*[J], 1984, 21(1-2):

- 89  
22 Huin D, Flauder P, Leblond J B. *Oxidation of Metals*[J], 2005, 64(1-2): 131  
23 Inden G. *Materials Issues for Generation IV Systems*[M]. Berlin: Springer, 2008: 73  
24 Chen R Q, Zou C W, Yan X D et al. *Thin Solid Films*[J], 2011, 519(6): 1837  
25 Kim K M, Yeom J T, Lee H S et al. *Thermochimica Acta*[J], 2014, 583: 1

## 低氧分压下 NiTi 记忆合金的氧化行为

邵明增<sup>1,2</sup>, 赵旭<sup>1,2</sup>, 杨洪波<sup>1,3</sup>

(1. 西安建筑科技大学, 陕西 西安 710055)

(2. 陕西省黄金与资源重点实验室, 陕西 西安 710055)

(3. 陕西省冶金工程技术研究中心, 陕西 西安 710055)

**摘要:** 研究了 NiTi 形状记忆合金在 H<sub>2</sub>-H<sub>2</sub>O 气氛下 400~700 °C 的氧化行为。合金的氧化过程遵循立方规律, 氧化激活能 127.52 kJ/mol。氧化显著降低了试样表面的 Ni 含量。400 °C 氧化的试样, 其表面形貌与其他试样不同, 并且氧化膜太薄, 截面结构无法用 SEM 分析。500、600、700 °C 氧化的试样, 表面有 2 种形貌的氧化物, 一种是颗粒状氧化物, 另一种是晶须状氧化物。截面分析表明, 氧化膜分为两层, 上层由 TiO<sub>2</sub> 构成, 下层由 Ni<sub>3</sub>Ti 构成, 两层界面处有孔洞生成。

**关键词:** NiTi 合金; 选择氧化; 低氧分压; TiO<sub>2</sub>

---

作者简介: 邵明增, 男, 1984 年生, 博士, 讲师, 西安建筑科技大学冶金工程学院金属材料系, 陕西 西安 710055, 电话: 029-82202923, E-mail: smz516@163.com